Double transition metal MXenes with wide band gaps and novel magnetic properties

SCHOLARONE™
Manuscripts

Journal Name

ROYAL SOCIETY OF CHEMISTRY

ARTICLE TYPE

Double transition metal MXenes with wide band gaps and novel magnetic properties†

Weiwei Sun,[a] Yu Xie,[a] and Paul R. C. Kent [a,b]

Novel wide band gaps and magnetism in ordered titanium-vanadium, titanium-chromium, and titanium-manganese carbide and nitride based MXenes are predicted using density functional theory. Based on the recent synthesis of Ti centred double transition metal MXenes, we study MXenes with a central Ti layer and different surface early $3d$ metals, and various terminations, TiM_2X_2T (M=V, Cr, Mn; X=C, N; T=H, F, O, OH). While previously studied MXenes are strongly metallic, we predict surface metal and termination dependent metal-insulator transitions in the Cr-N and Mn-N series. A uniquely wide band gap over 1 eV is predicted for $TiMn_2N_2F_2$ using the HSE06 density functional while the unterminated $TiMn_2N_2$ remains metallic. The entire $TiCr_2C_2T$ series is predicted to be semiconducting. Distinct from the more common Ti-C MXenes, not all combinations of metals and terminations are predicted to be stable. Within the examined sets of materials, anti-ferromagnetic orders are generally most favorable. The new MXenes further extend the range of properties accessible in this family of two-dimensional nanomaterials.

1 Introduction

The MXenes are two-dimensional (2D) transition metal carbides and nitrides, which are excellent candidates for numerous energy storage, energy conversion, catalysis, and device applications due to their excellent stability, electrical conductivity and capacitive and redox-based energy storage capacities[1–6]. More than 20 MXenes with different transition metals and numbers of atomic layers have been synthesized to-date[3,7,8]. These are primarily single transition metal MXene carbides. Very recently, metallic 2D nitrides such as Mo_2N and W_2N and V_2N were synthesized by novel methods[9,10]. However, compared to the better known carbides, the number of synthesized nitrides is small, and the range of accessible properties and how they may differ from the carbides is not known. Ordered double transition metal MXenes such as $Mo_2TiC_2T_x$, $Mo_2Ti_2C_3T_x$, and $Cr_2TiC_2T_x$ have also been

predicted and synthesized.[11–13] Their unique "sandwich" structures with both outer and inner metal layers gives a new route to tuning MXene properties. The combination of both double metals and mixed carbon-nitrides potentially greatly expands the range of accessible properties and applications.

Computational studies on MXenes have expanded rapidly.[14] Although the most common MXenes such as Ti_3C_2 are metallic and non-magnetic, a few MXenes have different electronic and magnetic structures. The Mn centered double transition metal MXenes have been investigated by Dong *et al.*[15], and high magnetic moments up to 4 μ_B/unit cell and high Curie temperatures up to 1133 K were reported. The established investigations of magnetism of MXenes have focused on the single metal MXene. For example, some display high electron population at the Fermi level (ε_f), indicating a preference towards spin-polarization according to the Stoner criteria. In the asymmetrically functionalized Cr_2C, a Néel temperature as high as 400 K has been predicted, whose bipolar antiferromagnetic (AFM) state can be tuned into half-metallic AFM by electron or hole doping.[16] Si *et al.* have predicted that unterminated Cr_2C is a ferromagnetic (FM) half-metal, whereas both FM and half-metallicity disappear with surface terminations.[17] Half-metallic Ti_2NO_2 and Cr_2NO_2 were predicted to have usually high magnetic moments and high Curie temperatures (up to 9 μ_B/unit cell and 1877 K).[18] Strain driven metal-insulator and magnetic ordering transitions are predicted in M_2C MXenes.[19] These results suggest that by exploiting a wide compositional freedoms of the double metal MXenes, we may reach additional novel magnetic, half-metallic, or insulating

behaviors at zero strain and with readily experimentally achievable surface terminations.

In this study, we focus on the group of Ti centered double transition metal MXenes (TiM_2X_2T) [11] We consider surface metals M of V, Cr, Mn and the anion sites X of C, N; and the four terminations T of H, O, F, OH, and unterminated (bare) surfaces. On the basis of this systematic study, the evolution of the structures, magnetic orders, and electronic structure is computationally established. We predict several materials with properties that are not found in the single metal ion and carbide family of MXenes including various magnetic orders, near half-metallicity, a semiconducting bare MXene, and termination controlled metal-insulator transitions.

2 Computational methods

Density functional theory (DFT) simulations are carried out using the Vienna ab initio simulation package (VASP),[20–22] within the projector augmented wave (PAW)[23,24] approach. Spin-polarized DFT+U calculations were used for all calculations,[25] using the exchange-correlation functional parameterized by Perdew, Burke, and Ernzerhof (PBE)[26] and on-site Coulomb term U values for Ti, V, Cr, and Mn of 0, 4.0[27], 4.0[28,29], 4.0[18] eV, respectively, with a fixed exchange parameter J of 1.0 eV. The 3d and 4s states were considered as the valence electronic configuration for Ti, V, Cr and Mn with the frozen semi-core 3s and 3p states. For C and N, the 2s and 2p states were treated as the valence states. A cut-off energy of 550 eV was used in all calculations, and the convergence criteria were set to be 10^{-7} eV for the total energy and 1×10^{-2} eV/Å for forces. We simulated isolated MXene sheets by including a 15 Å vacuum layer between neighboring images. Brillouin zone integrations were performed using the Methfessel-Paxton method[30] with a width of 0.05 eV. We considered several possible magnetic ground states including a ferromagnetic (FM) and three anti-ferromagnetic (AFM) configurations. The tested AFM configurations are shown in Fig. 1. All magnetic configurations were simulated using a 2×1 supercell and $7 \times 13 \times 1$ Γ centered **k**-point meshes to obtain an energy convergence of 1 meV per atom. For computation of the density of states and other ground state properties, a denser **k** mesh sampling by $13 \times 19 \times 1$ grids was used at the fully relaxed geometry. The obtained favorable magnetic orders were double-checked within a 2×2 supercell, and detailed discussions were addressed in the supplemental information(SI) on the basis of Fig. S2. It can be concluded that the currently adopted 2×1 supercell is sufficient for the majority of MXenes. The dynamical stabilities of all studied thirty MXenes were examined using the finite displacement method implemented in the PHONONPY software[31]. We used $2 \times 4 \times 1$ supercells and $5 \times 5 \times 1$ **k**-point meshes to manage overall computational cost. Only the Cr and Mn based MXenes, where there contain several semiconductors attracting more interests have been presented in the main text. The Vanadium based MXenes are reported in SI Fig. S1 because of the fact that few stable structures are stable.

Due to the uncertainties associated with the DFT+U method, we also performed a limited number of Heyd-Scuseria-Ernzerhof (HSE06) hybrid functional[32–34] calculations. Although significantly more computationally expensive, hybrid functionals provide more reliable energetics and band gaps.[32,35] As described below, the $TiCr_2C_2$ and $TiMn_2N_2$ series are particularly interesting, and we performed full geometric relaxation as well as electronic structure analysis with the hybrid functionals. Due to the higher cost of the calculations, k-point grids were reduced to $4 \times 4 \times 1$ Γ centered k-point meshes in structural optimization, and dense $6 \times 6 \times 1$ Γ meshed were used for electronic structure calculations. These were sufficient to converge the total energy to 10 meV.

3 Results

3.1 Dynamical stability

To ensure that the newly predicted MXenes are structurally stable, we first calculated the phonon density of states (PH-DOS), as shown in Fig. 2. In contrast to the well-studied Ti-C based MXenes, several combinations were found to be dynamically unstable, displaying phonons at negative frequencies. In addition, five out of thirty structures are absent because we were unable to converge all necessary displacement calculations to self-consistency, which we have also taken as an indication of structural instability due to large changes in the electronic and/or magnetic structure. We also identify several materials with only slightly negative phonons, such as bare $TiCr_2N_2$ and $TiMn_2C_2$ and $TiMn_2C_2F_2$. These could potentially be stabilized, e.g., by applying strain, as have been investigated and proven effective Mo_2C.[36] A reduction of systematic error in the phonon calculation through use of larger supercells, or consideration of mixed termination, beyond the scope of this study, could also result in stabilization. Given these considerations, we find a total sixteen of (quasi) stable MXenes: the O terminated TiV_2C_2 (1); H and OH terminated TiV_2N_2 (2); the entire $TiCr_2C_2$ series (5), the bare, O, OH terminated $TiCr_2N_2$ (3); the bare and F terminated $TiMn_2C_2$ (2); and the bare, H, F terminated $TiMn_2N_2$ (3). The clearly unstable MXenes are excluded in any discussions below.

Fig. 1 The three studied AFM magnetic orders type I (a), II (b), and III (c). The side view and the top view are respectively shown in the upper and lower panels. Atom types are indicated by blue for Ti, black (majority spin) and purple (minority spin) for surface metals, and brown for either C or N (X), and red for terminations (T).
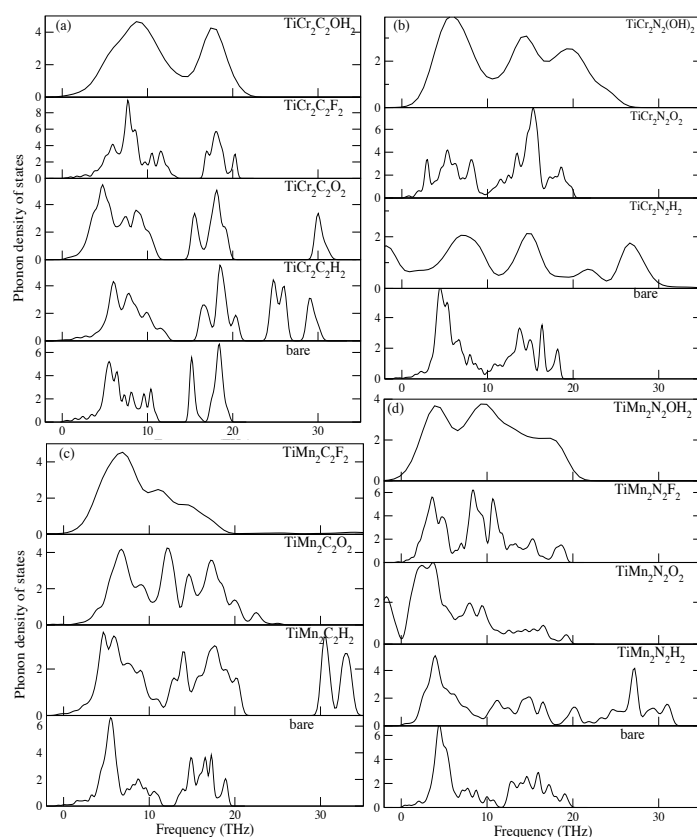
Fig. 2 Phonon density of states (PH-DOS) of MXenes of the series of (a) $TiCr_2C_2$, (b) $TiCr_2N_2$, (c) $TiMn_2C_2$ and (d) $TiMn_2N_2$.

3.2 Composition dependent ground states

Since the central Ti layer is (nearly) non-spin polarized, surface metals play the predominant role of determining the magnetic order. In the double transition metal MXene structures, the surface transition-metals are subject to an octahedral crystal field leading to a two bands splitting, i.e. lower band t_{2g} (d_{xy}, d_{yz}, and d_{xz}) and higher band e_g ($d_{x^2-y^2}$ and d_z^2). The trade off between crystal field splitting (CFS) and the Hunds rule determines the electronic occupation on 3d orbital, which counts the spin moment. Therefore, different configurations of 3d orbitals in metals give rise to distinct magnetic behaviors over the range of MXenes considered. Full details of the favorable magnetic order for each composition are given in Table **S1**.

The majority of MXenes are in AFM ground states, suggesting that the surface metals are mainly in super-exchange, which is a usually strong AFM coupling between two next-to-nearest neighbor cations through a non-magnetic anion (Ti). Another potential reason for the favorable AFM orders are when multiple types of interactions co-exist, the AFM one is generally dominant. The FM state is relatively rare and only found in F terminated $TiMn_2C_2$, where the spin moment of 16.3 μ_B per cell is found and the spin moment of each Mn site is about 4 μ_B. Note that such highly polarized MXenes are scarcely reported. Overall, the AFM coupling is the predominant magnetic interaction in studied MXenes, and the preferred magnetic order is composition and surface termination dependent.

As discussed earlier, varying the surface metals can vary the configuration of d orbitals. Externally, different functional groups or surface terminations can also modify the electronic and magnetic structure. The calculated spin moments for different terminations are shown in Fig. 3 (a). Note that the spin-polarized ions are surface metals and the central Ti ions are comparatively inert. Taking $TiCr_2N_2$ for example, it has been determined that Ti atoms are (nearly) non-spin polarized indicating that Ti has probably donated two electrons to N to diminish the unpaired electrons, leaving a valence configuration of [Ar]$d2$, in which the inert Ti atoms can be realized. This also implies that each N atom has a capability to accept two electrons from Cr leading it to a valence configuration of [Ar]$d4$. According to the Hunds rule the Cr should have 4μ_B for a maximum moment. Fig. 3 (a) shows that Cr spin moment is about 3.5 μ_B, close to the predicted value. Following this simple model, from V to Cr and ending up with Mn, and from C to N, the spin moments are expected to increase, and remarkably the trend is in a good agreement with the *ab initio* calculations in Fig 3 (a). Turning to the terminated MXenes, considerable changes occur after the chemical absorption of the terminations on the MXene surfaces. Following Hunds rule, the calculated spin moments shown in Fig. 3 (a) are in the line with these predictions but with some reductions. For the stable O terminated MXenes, O termination always suppresses the spin moment in the two series of Cr based MXenes compared with other limited number of terminated structures, clearly visible as the dip in Fig. 3 (a). We can deduce that O atoms with the oxidation states of -2 have a strong capability of attracting electrons from surface metal atoms, whose d electrons are reduced with the oxidation, and accordingly in turn reduce the maximum μ_s of surface metal atoms. Therefore, a steady increase of spin moment is realized by replacing with heavier cation or anion elements of MXenes, and the O termination is much likely to suppress the magnitude of spin-polarization of MXenes.
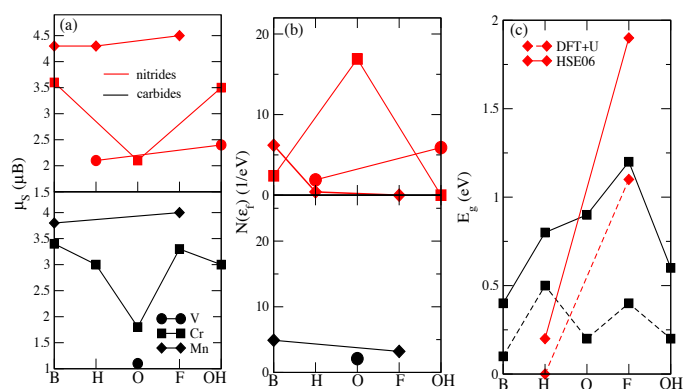
Fig. 3 The bare (B) and termination dependent (H, O, F, OH) (a) spin moments of surface metals (μ_S), (b) the DOS at the Fermi energy N(ε_f), and (c) band gaps of $TiCr_2C_2$ and $TiMn_2N_2$ series calculated in DFT+U (marked as dashed lines) and HSE06 (marked as solid lines) functionals. The lines are guide to the eye only.

Proceeding to the plot of DOS(ε_f), we now characterize the metallicity of all the stable MXenes. Surprisingly, the entire series of $TiCr_2C_2$ is found to be semiconducting. The V based MXenes

all display low DOS(ε_f) implying they are poor metals. For the Cr-N series, the TiCr$_2$N$_2$(OH)$_2$ is found to be semiconducting. For the two stable Mn based carbides, both are metallic, while for the nitrides, both the F and OH terminated materials become semiconducting, in contrast to their metallic state when bare. The terminations play a strong and effective role is turning many of the bare metallic MXenes to semiconductors. Surprisingly we also discover one semiconducting bare MXenes-TiCr$_2$C$_2$, which is the first non-metallic bare MXene, to our knowledge.

For the semiconducting MXenes, the evolution of band gaps of TiCr$_2$C$_2$ and TiMn$_2$N$_2$ series are shown in Fig. 3 (c). Most uniquely, there is one bare MXene that is semiconducting, and there are many terminated MXenes with a sizable band gap. Data for both DFT+U and HSE06 are presented. Note that our HSE06 calculations we performed with full structural relaxation because we found that static calculations using DFT+U structures were associated with residual pressures of order 1 GPa and also residual forces of about 0.5 eV/Å.

We should point out that the bare TiCr$_2$C$_2$ is a semiconductor with a gap of 0.1 eV (DFT+U) and 0.4 eV (HSE06). The terminated MXenes are also semiconductors with wider band gap values ranging from 0.1 to 1.3 eV (DFT+U) and 0.4 to 1.9 eV (HSE06). Yang *et al.* have studied Cr$_2$M'C$_2$T$_2$(M'=Ti or V; T=O, OH, F) and showed that the AFM orders are more favorable in the Cr$_2$TiC$_2$ series by calculating electronic structure with hybrid functionals using PBE+U relaxed structures. [37]

It is worth noting that TiCr$_2$C$_2$ remains gapped in HSE06. All the previously computed DFT+U band gap values are enhanced in HSE06, which illustrates that the semiconducting behavior is robust. In the TiMn$_2$N$_2$ series, the termination dependent metal-insulator transition is also reproduced in HSE06. The only significant disagreement between DFT+U (with our chosen U values) and HSE06 takes place on H and O terminated TiMn$_2$N$_2$. Clearly empirical tuning of the DFT+U functional could bring about improved agreement if desired. Overall, the qualitative prediction of MXenes with significant band gaps are highly consistent between the two methods. Interestingly, the predicted band gaps extend into the optical spectrum, suggesting new applications for MXenes provided suitable carriers can be injected.

4 Discussion

4.1 Semiconducting MXenes

MXenes are well known to be excellent conductors, but as shown in Fig. 3, several semiconducting MXenes are identified, in particular, the bare TiCr$_2$C$_2$. By varying the surface metal or anion elements, we are able to compare the electronic structure of TiCr$_2$C$_2$ (semiconductor), TiCr$_2$N$_2$(metallic solution with one more 2p electron on the anion site than TiCr$_2$C$_2$) and TiMn$_2$C$_2$ (metallic solution with one more 3d electron on the surface metal than TiCr$_2$C$_2$) shown in Fig. 4(a-c) to unravel the origin of the fomation of the semiconducting TiCr$_2$C$_2$. It is clear that the chemical variation on either site will turn it to metal. On the basis of the DOS plot, the key consequences of TiCr$_2$C$_2$showing semiconducting nature are summarized as: (i) It has been well accepted that in both bulk TiC and Ti based MXenes, a valley-like DOS in

the vicinity of ε_f is formed[38,39], and this feature is maintained in TiCr$_2$N$_2$ and TiMn$_2$C$_2$ which makes the two structures metallic; (ii) the stronger bonding and anti-bonding states of Ti(3d)-C(2p) are more pronounced in TiCr$_2$C$_2$ than those in other MXenes, which strengthens the band splitting and helps form a band gap. Based on these findings, the presence of insulating solutions is attributed to the strong splitting of the central layer Ti-X interactions, as the surface metal states are (almost) semiconducting.

In addition to the intrinsically semiconducting TiCr$_2$C$_2$, we also found termination induced metal-insulator transitions in the TiCr$_2$N$_2$ and TiMn$_2$N$_2$ series. In the former, the introduced OH termination opens up a band gap of 0.5 eV (DFT+U), and in the latter, greater band gap of 1.2 eV (DFT+U) can be achieved by adding F termination shown in Fig. 4(d, f). To uncover the origin of metal-insulator transitions, we first characterize the termination induced changes by differentiating DOS of both bare and terminated MXenes and more importantly propose the principles of metal-insulator transition. For all three bare MXenes (see Fig. 4(b,c,e)), DOS of surface M layers are always in the low DOS at ε_f, and the metallic feature is mostly introduced by the central Ti-X layer. The bare TiCr$_2$N$_2$ and TiMn$_2$N$_2$ both have low DOS at ε_f, indicating these bare MXenes are poor metals, but for the two bare Mn based MXenes, there are small hump derived by Ti-3d states that differs from the "valley" DOS observed in the Cr based MXenes. Terminations can directly strengthen the surface M-3d orbital splitting and open up a gap in the surface M-T layer, while regarding the central Ti-N layer, the termination introduced effects are case dependent. One can deduce that TiCr$_2$N$_2$(OH)$_2$ is weakly modified by functionalizing terminations from Fig. 4(d), conversely a strong perturbation has been embedded into TiMn$_2$N$_2$F$_2$ (f), where now a stronger hybridization between N and Mn is present. Therefore, terminations can reduce the already low DOS at ε_f of the surface layer, and leads surface M layer and N to a stronger interaction, which simultaneously regulates the Ti-3d states. The band structure of TiCr$_2$N$_2$(OH)$_2$, TiMn$_2$N$_2$F$_2$ are also calculated and discussed in SI. Fig. S4. The factors discussed above together support the 3d-2p hybridization and further strengthen the splitting in both central and surface layers, which eventually results in the metal-insulator transition.

For the emerging semiconducting MXenes, there are a few structures exhibiting band gap values larger than 1 eV, which can be potentially used in the renewable energy generation, distribution and storage. Via analyzing the orbital decomposed DOS, we are able to give insights into the feature of the newly discovered semiconductors, e.g. Mott or charge-transfer insulator, and also provide the leading excitation mechanism. The M-3d states are both dominating in the band edges of the surface layer, and the leading N-2p (in the valence band) to Ti-3d (in the conduction band) excitation is present for the central layer. The selected two semiconducting MXenes are therefore charge-transfer semiconductors, and the layer dependent as well as inter-atomic band edge derived excitations are worthy of performing in-depth investigations for novel optical properties.
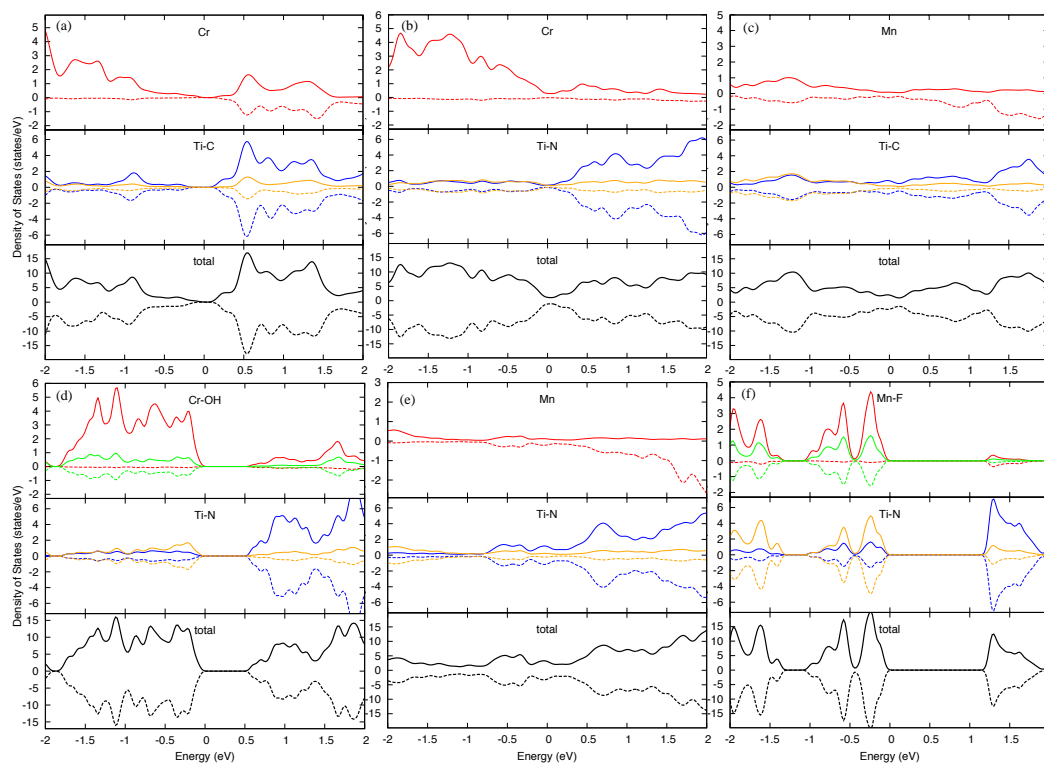
Fig. 4 The orbital projected DOS of (a) $TiCr_2C_2$, (b) $TiCr_2N_2$, (c) $TiMn_2C_2$, (d) $TiCr_2N_2(OH)_2$, (e) $TiMn_2N_2$, and (f) $TiMn_2N_2F_2$. On the top panel, the DOS of surface metal M-3d colored in red is presented; on the middle panel, the central Ti-3d and the X-2p states (X=C/N) colored in blue and orange are displayed respectively; and on the bottom, the total DOS colored in black is plotted. All plots are aligned with ε_f at 0 eV.

4.2 Magnetic interactions

The magnetic interactions of double metal MXenes differs should differ from the well-known M_2X MXenes due to the distinct coordination of the atoms. To analyze the exchange couplings and energies we use a Heisenberg spin Hamiltonian:

- $E_{FM} = E_0 - (6J_1 + 3J_2 + 3J_3)|S|^2$

- $E_{AFM-I} = E_0 - (6J_1 - 3J_2 - 3J_3)|S|^2$

- $E_{AFM-II} = E_0 - (-2J_1 + J_2 - 3J_3)|S|^2$

- $E_{AFM-III} = E_0 - (-2J_1 - J_2 + 3J_3)|S|^2$

where J_1, J_2, J_3 are the exchange interactions between the first nearest neighbors (NN), the second NN, the third NN. For the considered four possible magnetic ground states: FM, AFM-I, AFM-II, and AFM-III shown in Fig. 1. With the above spin Hamiltonian, one can easily calculate the magnetic exchange parameters that can be used to estimate the Néel/Curie temperature and/or further to perform spin dynamics. One stable near half-metal ferromagnetic $TiMn_2C_2F_2$ is identified, and the electronic structure can be found in Fig. S2. The near half-metallic ferromagnetic $TiMn_2C_2F_2$ has a lowering of energy of 0.357, 0.532, 0.682 eV with respect to the AFM-I, II, III configurations. The magnetic interaction parameters J_{ij} from the nearest to the farthest are respectively 4.449, 5.332, and 0.322 meV, which indicates a Curie temperature of 637 K in the mean-filed approximation of $\frac{2}{3}S(S+1)\sum_{i\neq 0}J_{0i}/k_B$ [40].

While theoretical studies usually focus on single terminations, in reality, and with current synthesis techniques, a variety of combinations are often measured [41]. To assess whether the novel predicted properties may be maintained with mixed terminations, we considered the two semiconducting $TiCr_2C_2$ and $TiMn_2N_2$ series functionalized by combinations of O and F, O and OH are used. Due to the use of finite supercells, the mixed terminations are necessarily ordered. All DOS of bi-termination functionalized MXenes are plotted in Fig. S3 (b). $TiCr_2C_2O(OH)$ is metallic, and $TiCr_2C_2OF$ is a half-metal; while both $TiMn_2N_2OF$ and $TiMn_2N_2O(OH)$ are half-metallic. This demonstrates that additional studies and considerations of mixed terminations are warranted, as are methods to prepare and characterize MXenes with desired terminations.

5 Conclusions

Double transition metal MXenes with a Ti central layer and various surface metal and cationic layers have been investigated by means of density functional theory. The terminations and different cationic configurations lead to diverse magnetic orders, and properties distinct from the well-studied single transition metal carbides. Oxygen terminations lead MXenes to least spin moment, while a stronger crystal field splitting with the hydrogen termination reduces the magnitude of polarization. An intrinsic semiconducting MXene $TiCr_2C_2$ is discovered and characterized with a band gap of 0.1 eV (DFT+U) or 0.4 eV (HSE). With appropriate surface termination, several metallic MXenes can be made semiconducting, such as $TiMn_2N_2$, where a uniquely large

gap for $TiMn_2N_2F_2$ of 1.1 eV (DFT+U) or 1.9 eV (HSE06) is predicted. The termination induced metal-insulator transition in MXenes suggests possible sensing and device applications. The newly predicted MXenes significantly extend the range of properties achievable in this family of materials, and we encourage experimental studies.

6 Acknowledgments

References

1 Y. Xie and et al., *J. Am. Chem. Soc.*, 2014, **136 (17)**, 6385–6394.

2 M. R. Lukatskaya, B. Dunn and Y. Gogotsi, *Nat. Commun.*, 2016, **7**, 12647.

3 B. Anasori, M. R. Lukatskaya and Y. Gogotsi, *Nat. Rev. Mater.*, 2017, **2**, 16098.

4 M. Naguib and et al., *ACS Nano*, 2012, **6**, 1322–1331.

5 X. Zhang, ZiheZhang and ZhenZho, *J. Energy Chem.*, 2018, **27**, 73–85.

6 B. Anasori, M. R. Lukatskaya and Y. Gogotsi, *Nat. Rev. Mat.*, 2017, **2**, 16098.

7 M. Naguib and Y. Gogotsi, *Acc. Chem. Res.*, 2015, **48**, 128–135.

8 M. Naguib and et al., *Adv. Mater.*, 2011, **23**, 4248–4253.

9 P. Urbankowski and et al., *Nanoscale*, 2017, **DOI:**, 10.1039/C7NR06721F.

10 X. Xiao and et al., *ACS Nano*, 2017, **11 (2)**, 2180–2186.

11 B. Anasori and et al., *ACS Nano*, 2015, **9 (10)**, 9507–9516.

12 B. Anasori and et al., *Nanoscale Horiz*, 2016, **1**, 227–234.

13 T. L. Tan, H. M. Jin, M. B. Sullivan, B. Anasori and Y. Gogotsi, *ACS Nano*, 2017, **11 (5)**, 4407–4418.

14 M. Khazaei, A. Ranjbar, M. Arai, T. Sasaki and S. Yunoki, *Journal of Materials Chemistry C*, 2017, **5**, 2488–2503.

15 L. Dong, H. Kumar, B. Anasori, Y. Gogotsi and V. B. Shenoy, *J. Phys. Chem. Lett.*, 2017, **8 (2)**, 422–428.

16 J. He, P. Lyu, L. Z. Sun, A. M. Garca and P. Nachtigall, *J. Mater. Chem. C*, 2016, **4**, 6500–6509.

17 C. Si, J. Zhou and Z. Sun, *ACS Appl. Mater. Interfaces*, 2015, **7**, 17510–17515.

18 H. Kumar, N. C. Frey, L. Dong, B. Anasori, Y. Gogotsi and V. B. Shenoy, *ACS Nano*, 2017, **11**, 7648–7655.

19 G. Gao, G. Ding, J. Li, K. Yao, M. Wu and M. Qian, *Nanoscale*, 2016, **8**, 8986–8994.

20 G. Kresse and J. Hafner, *Phys. Rev. B*, 1993, **48**, 13115.

21 G. Kresse and J. Hafner, *Phys. Rev. B*, 1994, **49**, 14251.

22 G. Kresse and J. Furthmuller, *Phys. Rev. B*, 1996, **54**, 11169.

23 P. E. Blöchl, *Phys. Rev. B*, 1994, **50**, 17953.

24 G. Kresse and D. Joubert, *Phys. Rev. B*, 1999, **59**, 1758.

25 S. L. Dudarev, S. Y. Savrasov, C. J. Humphreys and A. Sutton, *Phys. Rev. B*, 1998, **57**, 1505–1509.

26 J. P. Perdew, K. Burke and M. Ernzerhof, *Phys. Rev. Lett.*, 1996, **77**, 3865.

27 J. Hu, B. Xu, C. Ouyang, S. A. Yang and Y. Yao, *J. Phys. Chem. C*, 2014, **118**, 24274–24281.

28 J. He, S. Ma, P. Lyu and P. Nachtigall, *J. Mater. Chem. C*, 2016, **4(13)**, 2518–2526.

29 W. B. Zhang, Q. Qu, P. Zhu and C. H. Lam, *J. Mater. Chem. C*, 2015, **3**, 12457–12468.

30 M. Methfessel and A. T. Paxton, *Phys. Rev. B*, 1989, **40**, 3616.

31 A. Togo and I. Tanaka, *Scr. Mater.*, 2015, **108**, 1–5.

32 J. Heyd, G. E. Scuseria and M. Ernzerhof, *J. Chem. Phys.*, 2001, **118**, 8207.

33 M. M. J. Paier, K. Hummer, G. Kresse, I. C. Gerber and J. G. Ángyán, *J. Chem. Phys.*, 2006, **124**, 154709.

34 J. Heyd, G. E. Scuseria and M. Ernzerhof, *J. Chem. Phys.*, 2006, **219906**, 124.

35 V. Eyert, *Phys. Rev. Lett.*, 2011, **107**, 016401.

36 W. Sun, Y. Li, B. Wang, X. Jiang, M. Katsnelson, P. Korzhavyi, O. Eriksson and I. D. Marco, *Nanoscale*, 2015, **8**, 15753–.

37 J. Yang, X. Zhou, X. Luo, S. Zhang and L. Chen, *App. Phys. Lett.*, 2016, **109**, 203109.

38 W. Sun, H. Ehteshami and P. A. Korzhavyi, *Phys. Rev. B*, 2015, **91**, 134111.

39 Y. Xie and P. R. C. Kent, *Phys. Rev. B*, 2013, **87**, 235441.

40 M. Pajda, J. Kudrnovský, I. Turek, V. Drchal and P. Bruno, *Phys. Rev. B*, 2001, **64**, 174402.

41 H.-W. Wang, M. Naguib, K. Page, D. J. Wesolowski and Y. Gogotsi, *Chem. Mater.*, 2016, **28(1)**, 349–359.